Propagation of ultracold atoms through bends in waveguides

M. W. J. Bromley* and B. D. Esry†
Department of Physics, Kansas State University, Manhattan, Kansas 66506, USA
(Received 21 July 2003; published 9 October 2003)

The properties of noninteracting, low-energy atom waves propagating through circular bends are investigated. Time-independent quantum mechanical calculations using various simple harmonic oscillator based confining potentials explore the transmission, reflection, and mode-transfer probabilities over a range of energies. It is shown that at low energies single-mode wave propagation dominates. At higher energies, however, excitation and transmission of other modes become significant. Notably, reflections generally remain negligible even for sharply curved bends. The behavior near the mode thresholds and their associated resonances is emphasized.

DOI: 10.1103/PhysRevA.68.043609 PACS number(s): 03.75.Be, 03.75.Kk, 03.65.Ge, 39.25.+k

I. INTRODUCTION

Recent years have seen exciting advances in the size of the ultracold atomic physics playground. The ability of experimentalists to trap and transport atoms above microchip surfaces [1], in magnetic guides [2], and among optical elements [3,4] is opening up a vista of atomic physics opportunities both fundamental and practical [5–7].

Given the volume of experimental ''atom chip'' research, and that the basic principles are now well known [8–13], there are surprisingly few theoretical investigations. Recent fundamental studies have focused on understanding heating and decoherence loss during matter wave propagation above a surface [14–16], and conditions for adiabatic wave-packet propagation through micrometer scale potentials [17,18]. Theoretical studies of specific atom chip devices include focusing an atomic beam [19], quantum point contacts [20], interferometers [21–24], in-coupling (loading precooled atoms onto the chip) [25,26], as well as a QED scheme for single-atom detection [27].

While matter wave optics requires all of the analogs of electromagnetic optical elements, it is also important to produce efficient guides to transport atoms between one component and the next in a confining potential to avoid diffraction. For the present paper we investigate the second simplest atom optical element, the circular waveguide bend. Bends have been investigated experimentally [28] and theoretically [29]. These studies, however, involved atoms at high temperatures (i.e., propagation velocities on the order of 10 m/s and de Broglie wavelengths much less than the characteristic transverse trapping scales), so that the motion of atoms through the waveguide could be described classically.

The success of recent experiments in creating Bose-Einstein condensates (BEC's) above microchip surfaces [30–33] as well as their controlled, single-mode (excitationless) propagation [34–36] is rapidly heading toward full, ''on chip'' coherent control of matter waves. In this work we are primarily interested in single-mode propagation of low-energy atom waves with atomic densities such that atom-atom interactions can be neglected and the (linear) Schrödinger equation is applicable. This is the regime of particular interest to experimentalists investigating atom interferometry [7]. Previously, stationary solutions of a BEC propagating through a circular bend were obtained by solving the (nonlinear) Schrödinger equation using a weak attractive potential to approximate the effect of a circular bend [37]. Some of the limitations of this approximation are discussed in this paper.

As far as the fundamental wave mechanics is concerned, much can be learnt from the extensive literature on acoustic, electromagnetic, and electron waveguides and devices. For example, it is well known that hard-walled quantum bends [38,39] and bulges [40] with Dirichlet boundary conditions when connected to *infinite* leads possess bound states that do not exist classically. For the present paper we borrow heavily from the physics previously seen in studies of ballistic electron propagation through waveguide bends [41–43]. From a theoretical point of view, the circular bend results in a separable time-independent problem. This allows for an uncomplicated examination of the quantum mechanics of a circular bend, in particular, an investigation of the range of energies where single-mode wave propagation is maintained through bends with different confining potentials. Since most atom chip devices will demand the guiding of atoms through a bent potential of some form, the results of this paper should also apply more broadly.

II. DETAILS OF THE CALCULATIONS

Here we consider atoms that are prepared in a magnetic weak-field-seeking state and are trapped above the surface in a two-dimensional magnetic potential minimum resulting from wires laid out on a planar substrate. While there are a variety of experimental wire configurations in use [1,11], we consider only a wire configuration that does not require a bias magnetic field established across the entire atom chip surface. It is well known that a global bias field raises and lowers the potential minima as atoms propagate through a bent waveguide [28,29]. Experimentally, this is avoided by using multiwire configurations where the bias field is generated locally by the wires lying parallel to the main guiding wire(s), and thus the bias field tracks through the bend with-

*Electronic address: bromley@phys.ksu.edu
†Electronic address: esry@phys.ksu.edu

out affecting the potential minima.

To keep the model simple and general we also choose to neglect a bias field in the direction of propagation, which means that in principle the individual atoms composing the matter wave are susceptible to Majorana transitions. These transitions can occur when atoms traverse a magnetic-field-free region of space (i.e., the center of the waveguide). During this time there is some probability that the atomic spin will flip from a weak-field-seeking state to a strong-field-state, so that the atom is no longer trapped in the guide. While this would be a significant loss mechanism, there are many such experimental difficulties currently identified for ultracold atoms propagating above a room temperature surface [1,15]. For the present paper, we simply choose to ignore all such effects, maintaining the emphasis on the wave mechanics.

The removal of global bias fields simplifies our theoretical approach considerably; we need not consider any variation of the strength of the guiding potential either perpendicular to or parallel with the motion of the atoms. Consequently, the waveguide potentials are separable between the direction of propagation and the two transverse directions. Dividing space into the three regions shown in Fig. 1, the connecting leads are described by Cartesian coordinates (x,y,z), and the circular bend by polar coordinates (ρ,y,ϕ). The origin is at the same point for all regions, and the bend curves in the (x,z) and (ρ,ϕ) planes through an angle ϕ_0.

In keeping with our simplifications regarding the bias fields, we consider an idealized trapping potential. In practice, guiding potentials are quadratic near the minima at ρ_0 and $y=0$, so we employ simple harmonic oscillator (SHO) potentials:

$$
\begin{aligned}
V_{\mathrm{I}}(x,y,z) &= V_x(x)+V_y(y) \\
&= \frac{1}{2}m\omega^2[(x-\rho_0)^2+\lambda_y^2 y^2], \quad z\leqslant 0, \\
V_{\mathrm{II}}(\rho,y,\phi) &= V_x(\rho)+V_y(y) \\
&= \frac{1}{2}m\omega^2[(\rho-\rho_0)^2+\lambda_y^2 y^2], \quad 0\leqslant\phi\leqslant\phi_0, \\
V_{\mathrm{III}}(x',y,z') &= V_x(x')+V_y(y) \\
&= \frac{1}{2}m\omega^2[(x'-\rho_0)^2+\lambda_y^2 y^2], \quad z'\geqslant 0.
\end{aligned}
\tag{1}
$$

The present treatment is limited to cases in which the transverse spread of the wave function is smaller than ρ_0. In fact, the wave function is excluded from the shaded region of Fig. 1 by imposing infinite hard wall boundary conditions. The width of the vertical dimension of the waveguide (in y) is similarly chosen. For the results to be as general as possible, oscillator units are used throughout the rest of this paper. Energies are given in units of $\hbar\omega$, while lengths are in units of the oscillator width $\sqrt{\hbar/m\omega}$.

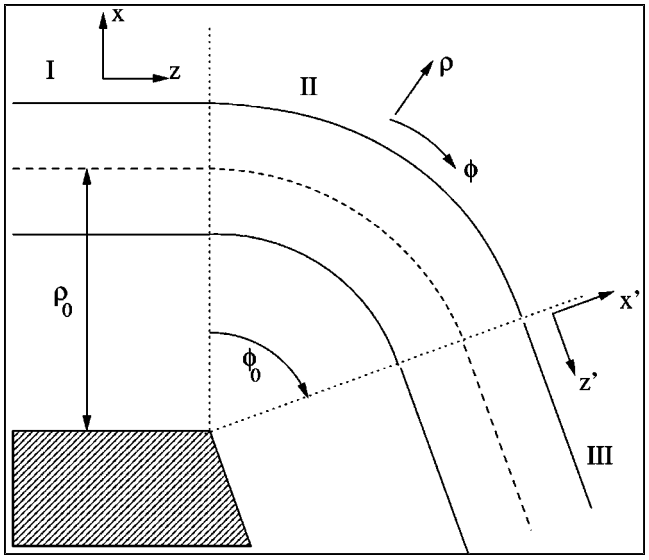

FIG. 1. Coordinate definitions for the three regions (I,II,III) of a two-dimensional bend through an angle ϕ_0. The dashed line at a distance of ρ_0 denotes the SHO potential minimum. The shaded area denotes the region that the interface matching method cannot sensibly describe.

As the guiding potential of Eq. (1) is separable, so is the Schrödinger equation in each region. All of the physics—mode mixing, reflection, etc.—is thus entirely a result of matching multichannel wave functions at the boundaries between regions. We perform this time-independent matching in essentially the same manner as can be found in nearly every quantum mechanics text for one-dimensional (1D) problems. Such matching has been described previously in the context of ballistic electron transport through 2D quantum wires [41,43–45], so a brief description is given here as it extends to a 3D waveguide. The wave functions in each region are constructed using plane waves as

$$
\begin{aligned}
\Psi_{\mathrm{I}}(x,y,z) &= \sum_\alpha \Phi_\alpha(x,y)[a_\alpha e^{ik_\alpha z}+b_\alpha e^{-ik_\alpha z}], \\
\Psi_{\mathrm{II}}(\rho,y,\phi) &= \sum_\beta \Theta_\beta(\rho,y)[c_\beta e^{i\kappa_\beta\phi}+d_\beta e^{-i\kappa_\beta\phi}], \\
\Psi_{\mathrm{III}}(x',y,z') &= \sum_\alpha \Phi_\alpha(x',y)[g_\alpha e^{ik_\alpha z'}+h_\alpha e^{-ik_\alpha z'}].
\end{aligned}
\tag{2}
$$

The transverse eigenstates of the two leads, $\Phi_\alpha(x,y)=\zeta_{n_x}(x)\xi_{n_y}(y)$, are determined from the eigenvalue equations

$$
\begin{aligned}
\left[-\frac{1}{2}\frac{d^2}{dx^2}+V_x(x)\right]\zeta_{n_x}(x) &= E_{n_x}\zeta_{n_x}(x), \\
\left[-\frac{1}{2}\frac{d^2}{dy^2}+V_y(y)\right]\xi_{n_y}(y) &= E_{n_y}\xi_{n_y}(y),
\end{aligned}
\tag{3}
$$

which are solved using a basis of B splines. Thus for a given total energy E the $\alpha=(n_x,n_y)$ lead mode has $k_\alpha^2=2(E-E_{n_x}-E_{n_y})$. For $k_\alpha^2>0$ the mode propagates, with the (known) incoming flux of that mode given by $k_\alpha|a_\alpha|^2$ and $k_\alpha|h_\alpha|^2$. Both $k_\alpha|b_\alpha|^2$ and $k_\alpha|g_\alpha|^2$ correspond to the (unknown) outgoing flux of the $k_\alpha^2>0$ mode. For evanescent modes $k_\alpha^2<0$, which demands $a_\alpha=h_\alpha=0$, while b_α and g_α are the (unknown) coefficients of the exponential decay outward from the bend. Defining the number of horizontal lead modes as N_x and the number of vertical modes as N_y, then the combined number of lead modes included in each calculation is $N_\alpha=N_xN_y$. Since in our simplified model the potential in the vertical direction $V_y(y)$ is the same throughout the leads and the bend, the quantum number n_y is a good quantum number and is thus conserved.

In polar coordinates, the bend Schrödinger equation is separable [41], and the $\beta=(n_\rho,n_y)$ bend transverse eigenstates $\Theta_\beta(\rho,y)=\varphi_{n_\rho}(\rho)\xi_{n_y}(y)$ are determined for each $n_y\in[0,N_y-1]$ by solving

$$\left[-\frac{1}{2}\left(\frac{d^2}{d\rho^2}+\frac{1}{\rho}\frac{d}{d\rho}\right)+(V_x(\rho)-(E-E_{n_y}))\right]\varphi_{n_\rho}(\rho)=-\frac{\kappa_{n_\rho}^2}{2}\frac{\varphi_{n_\rho}(\rho)}{\rho^2}. \tag{4}$$

The resultant eigenvalues are $-\kappa_\beta^2/2$, and the quantity $\hbar\kappa_\beta$ is the angular momentum of each mode in the bend (to a good approximation it is given by $\hbar\kappa_\beta\approx\hbar k_\beta\rho_0$). Note that the angular momentum need not be quantized since the bend subtends an angle less than 2π. This implies that the usual single-valued condition on the wave function is absent; instead, the total energy E is fixed and then κ_β is determined. While the exact eigensolutions of Eq. (4) for a hard walled bend with $V_x(\rho)=0$ are known to be Bessel functions [39], the solutions with harmonic confinement are not known. Equation (4) is thus solved numerically using a B-spline basis. The number of bend modes included in each calculation is $N_\beta=N_\rho N_y$. The infinite hard wall boundary conditions in ρ are applied at $\rho=\pi$ and $\rho=2\rho_0-\pi$, ensuring that the wave function of each region is well defined at the inner waveguide boundary.

To determine the $2N_\alpha+2N_\beta$ unknown coefficients of Eq. (2) (i.e., $\{b_\alpha\}$, $\{g_\alpha\}$, $\{c_\beta\}$, and $\{d_\beta\}$), the wave functions and their first derivatives are matched at interface I-II:

$$\Psi_{\rm I}(x,y,z)|_{z=0}=\Psi_{\rm II}(\rho,y,\phi)|_{\phi=0} \quad \text{and}$$

$$\left.\frac{\partial\Psi_{\rm I}(x,y,z)}{\partial z}\right|_{z=0}=\frac{1}{\rho}\left.\frac{\partial\Psi_{\rm II}(\rho,y,\phi)}{\partial\phi}\right|_{\phi=0}, \tag{5}$$

and also at interface II-III:

$$\Psi_{\rm III}(x',y,z')|_{z'=0}=\Psi_{\rm II}(\rho,y,\phi)|_{\phi=\phi_0} \quad \text{and}$$

$$\left.\frac{\partial\Psi_{\rm III}(x',y,z')}{\partial z'}\right|_{z'=0}=\frac{1}{\rho}\left.\frac{\partial\Psi_{\rm II}(\rho,y,\phi)}{\partial\phi}\right|_{\phi=\phi_0}. \tag{6}$$

These matching conditions are converted into manageable algebraic equations by substituting the expressions in Eq. (2) and projecting onto each of the N_α transverse lead wave functions $\Phi_\alpha(x,y)$. This projection produces $4N_\alpha$ equations which, when combined with the restriction $N_\alpha=N_\beta$, ensures a well-defined solution.

The final matching equations are succinctly displayed if we first define a series of matrices. The lead and bend momenta are grouped as

$$\underline{k}=\begin{pmatrix}k_1 & & & 0\\ & k_2 & & \\ & & \ddots & \\ 0 & & & k_{N_\alpha}\end{pmatrix} \quad \text{and}$$

$$\underline{\kappa}=\begin{pmatrix}\kappa_1 & & & 0\\ & \kappa_2 & & \\ & & \ddots & \\ 0 & & & \kappa_{N_\beta}\end{pmatrix}. \tag{7}$$

Also required are lead-bend overlap matrices $\underline{\chi}$ and $\underline{\chi'}$ with matrix elements

$$\chi_{\alpha\beta}=\langle\Phi_\alpha|\Theta_\beta\rangle \quad \text{and} \quad \chi'_{\alpha\beta}=\left\langle\Phi_\alpha\left|\frac{\Theta_\beta}{\rho}\right\rangle\right. . \tag{8}$$

As an example, we give the slightly strange interface matching integral

$$\chi'_{\alpha\beta}=\int\int\zeta_{n_x}(x)\xi_{n_y}(y)\varphi_{m_\rho}(\rho)\xi_{m_y}(y)/\rho\,dxdy, \tag{9}$$

where, due to the coordinate definitions, $x=\rho$ on the boundaries. The $4N_\alpha$ inhomogeneous linear equations are then written in matrix form as

$$\begin{pmatrix}-\underline{1} & \underline{0} & \underline{\chi} & \underline{\chi}\\ \underline{0} & -\underline{1} & e^{i\underline{\kappa}\phi_0}\underline{\chi} & e^{-i\underline{\kappa}\phi_0}\underline{\chi}\\ \underline{k} & \underline{0} & \underline{\kappa\,\chi'} & -\underline{\kappa\,\chi'}\\ \underline{0} & \underline{k} & -\underline{\kappa}e^{i\underline{\kappa}\phi_0}\underline{\chi'} & \underline{\kappa}e^{-i\underline{\kappa}\phi_0}\underline{\chi'}\end{pmatrix}\begin{pmatrix}\underline{B}\\ \underline{G}\\ \underline{C}\\ \underline{D}\end{pmatrix}=\begin{pmatrix}\underline{A}\\ \underline{k}\ \underline{H}\\ \underline{A}\\ \underline{k}\ \underline{H}\end{pmatrix}. \tag{10}$$

Although it was not indicated in Eq. (2), the coefficients actually carry an additional index to indicate the incident channel. The coefficients can then be organized into incom-

ing lead coefficient matrices $\underline{A}$ and $\underline{H}$, where each column corresponds to incidence in a different propagation channel. By symmetry, incidence from region I gives the same results as incidence from region III, so the incoming propagating modes are chosen to always be from region I, i.e., $\underline{H}=\underline{0}$. While we are specifically interested in propagation of the lowest mode [in which case $\underline{A}$ would simplify to the column vector $\mathbf{a}=(1,0,\ldots,0)$ of length N_α], we also calculate how the lowest N'_α states (with $k_\alpha^2>0$) propagate through the bend. Furthermore, the matrix elements are chosen as $A_{\alpha\alpha'}=\delta_{\alpha\alpha'}$, i.e., only single-mode incoming waves are considered in this paper. The unknown outgoing lead coefficients are grouped into the matrices $\underline{B}$ and $\underline{G}$, with the unknown bend coefficients grouped into $\underline{C}$ and $\underline{D}$. Each of the columns of these unknown matrices is a solution corresponding to a specific incoming mode given by each column of $\underline{A}$.

For the propagating modes in the lead (i.e., $k_\alpha^2>0$) the transmission and reflection probabilities are calculated as the ratio of the outgoing to the incoming flux, i.e.,

$$|\mathcal{T}_{fi}|^2=\frac{|g_f|^2k_f}{|a_i|^2k_i} \quad \text{and} \quad |\mathcal{R}_{fi}|^2=\frac{|b_f|^2k_f}{|a_i|^2k_i}. \tag{11}$$

As mentioned previously, n_y is conserved for the potentials of interest here. With no mode mixing between modes with different n_y, for simplicity, we adopt the notation $|\mathcal{T}_{fi}|^2=T^{n_y}_{n_{xf},n_{xi}}$ (with similar notation for reflection).

The computational limitations of this simple matching scheme as applied to electron transport through hard walled circular guides has been thoroughly investigated in the limit of tight bend curvature, and even for bend angles greater than 360°—"spiral"-type guides [43]. Essentially, numerical problems arise when including strongly closed channels (large $|\kappa_\beta|$) in the calculation, which generate exponentially large terms in the set of linear equations, restricting the extension of $(N_\alpha=)N_\beta\to\infty$. The ansatz used by Lin and Jaffe [43] offers one method for avoiding these difficulties. Nevertheless, we kept the simple matching scheme for two reasons. First, as the wave propagates through the bend, the centrifugal motion acts to push the wave function radially outward from $\rho=\rho_0$, but the SHO guiding potential works against this shift by localizing the propagating wave around $\rho=\rho_0$. Matching the disjointed eigenfunctions across the lead-bend interfaces is then somewhat less dramatic than is seen for the tight electron waveguide bends, and hence fewer channels are necessary in the present calculations for adequate convergence. Second, the maximum bend angle examined here is 180°, and since the exponential matrix elements of Eq. (10) contain $\kappa_\beta\phi_0$ terms, the exponential terms included in here are smaller than those required for the greater than 360° guides.

The transmission and reflection probability calculations were first validated for various geometries by repeating published 2D bend calculations [41,43,44,46]. Convergence of the numerical solutions with respect to the number of channels was monitored using the unitarity condition $\Sigma_f T^{n_y}_{n_{xf},n_{xi}}+R^{n_y}_{n_{xf},n_{xi}}=1$, for each of the initial modes. This condition was maintained at better than 1 part in 10^{10} for all calculations reported here.

TABLE I. The energy spectrum of the 1D eigenmodes transverse to the direction of wave propagation for a circular bend with an anisotropic 2D simple harmonic oscillator potential ($\lambda_y=0.64$) centered at $\rho_0=4\pi$. The horizontal lead (x), horizontal bend (ρ), and vertical (y) eigenmodes are separable, with up to 25 modes included in the calculations. All energies are given in oscillator units.

n	E_x(horiz)	E_y(vert)	E_ρ(horiz bend)
0	0.5000000	0.4000000	0.4992008
1	1.5000000	1.2000000	1.4991852
2	2.5000000	2.0000000	2.4991692
3	3.5000000	2.8000000	3.4991526
4	4.5000000	3.6000000	4.4991355
9	9.5000000	7.6000000	9.4990405
19	19.500000	15.600000	19.498788
24	24.500000	19.600038	24.498618

III. RESULTS

We focus primarily on the case $\phi_0=90°$ with $\rho_0=4\pi$, and the SHO potential used is anisotropic with $\lambda_y=0.64$ in Eq. (1). This choice is intended to mimic experimental atom chip configurations in which the confining magnetic potential is slightly weaker along the vertical direction (perpendicular to the chip surface) [1,11].

A. Eigenmodes

The energy eigenspectrum of this anisotropic potential is shown in Table I. For the leads, both the horizontal (x) and vertical (y) eigenmodes are simply those of a one-dimensional simple harmonic oscillator. The horizontal mode energies in the bend (ρ) are determined by setting $\kappa=0$ and

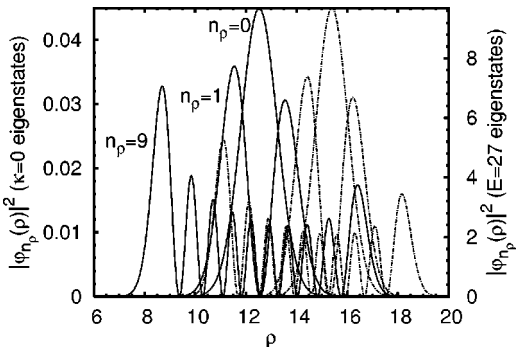

FIG. 2. The bend eigenfunction probability densities $|\varphi_{n_\rho}(\rho)|^2$ of Eq. (4) with $n_\rho=0,1,9$. Two sets of curves are given. First the solid lines are the threshold ($\kappa_{n_\rho}=0$) eigensolutions (the corresponding energy eigenvalues are given in the E_ρ column of Table I). Second, the dashed lines are the corresponding $E=27$ eigensolutions with the vertical mode fixed as $n_y=0$. Generally the bend eigenfunctions slosh outward as the energy is increased.

TABLE II. The combined 2D transverse (horizontal+vertical) energy thresholds of the lead and bend modes, given the same waveguide geometry as in Table I. Note that only modes with the same vertical number (n_y) can couple when propagating through the bend. All energies are given in oscillator units.

Mode (n_x,n_y)	E(lead)	E(bend)
0, 0	0.9000000	0.8992008
0, 1	1.7000000	1.6992008
1, 0	1.9000000	1.8991852
0, 2	2.5000000	2.4992008
1, 1	2.7000000	2.6991852
2, 0	2.9000000	2.8991692
9, 9	17.100000	17.098951
19, 19	35.100000	35.098788
24, 24	44.100038	44.098656

$E_{n_y}=0$ and finding the resultant eigenenergies of Eq. (4). These results are thus independent of n_y, and are also shown in Table I. The effect of having boundary conditions imposed is barely seen in the marginal deviation of the $n_y=24$ vertical mode eigenenergy from that of the ideal SHO eigenenergy.

To provide some idea of what the horizontal bend eigenfunctions look like, the threshold eigenfunctions ($\kappa=0$) are shown for $n_\rho=0,1,9$ as the solid lines in Fig. 2, bearing a similarity to the (not shown, but well known) $n_\rho=0,1,9$ ideal SHO solutions. However, the asymmetry of the threshold bend eigenfunctions in ρ is produced by the attractive $d/d\rho$ term in the Schrödinger equation in the bend [Eq. (4)]. The $n_\rho=0,1,9$ horizontal eigenfunctions for $E=27$ (with $n_y=0$) are shown as the dashed lines in Fig. 2. As the energy is increased, the bend eigenfunctions increasingly slosh outward from the SHO minima at $\rho_0=4\pi$. There is also an asymmetry in the $E=27$ eigenfunctions, i.e., $|\varphi_{n_\rho}(\rho)|^2$ is larger for $\rho<4\pi$ than for $\rho>4\pi$. This is due to the $E\neq 0$ eigenstate normalization, i.e., $\langle\varphi_{n_\rho}|1/\rho^2|\varphi_{n_\rho}\rangle=1$. Of importance for matching the wave functions, in which these bend functions are mapped onto lead SHO eigenfunctions $\zeta_{n_x}(x)$ that are perfectly symmetric and localized about $x=\rho_0$, even for low propagation energies the eigenstates in the bend significantly overlap with the center of the SHO waveguide.

The propagation threshold energy of each transverse mode corresponding to (n_x,n_y) in the leads and (n_ρ,n_y) in the bend is shown in Table II. It is evident in both Tables I and II that the energy of propagation in the bend is always slightly lower than that of the corresponding lead mode.

B. Bound states

That a bend connected to infinite leads supports a weakly bound state [38,39] can be understood from the bend lowering the energy thresholds relative to the leads. In other words, these bound states occur when a wave has enough energy to propagate in the bend ($\kappa_\beta^2>0$), but remains below the propagation threshold in the leads (i.e., $k_\alpha^2<0$). It has been found that 2D, hard walled, circular electron waveguides with an angle less than 360° support at most one bound state [43]. For the 3D case, since n_y is a good quantum number in our model, one bound state exists for each n_y, with the energy of each bound state located between the lead and the bend energy thresholds for the mode $(0,n_y)$. Moreover, because n_y enters Eq. (4) only to shift the zero of the energy, every bound state has the same binding energy.

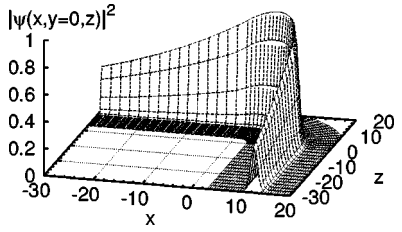

FIG. 3. The $n_y=0$ bound state probability density $|\psi(x,y,z)|^2$ of a 90° SHO bend with $\rho_0=4\pi$ taken as a slice through $y=0$. The bend, which is the region $x>0$ and $z>0$, is seen to have a symmetric (but very weakly bound) bound state, strongly confined to the position of the SHO minima at $\rho_0=4\pi$.

Each bound state calculation thus requires the condition $a_\alpha=h_\alpha=0$ for all modes. The $4N_\alpha\times 4N_\alpha$ matrix M in Eq. (10), however, cannot be diagonalized since E is manifested nonlinearly in the matrix elements. Thus, to solve the set of linear equations an additional constraint is required to ensure that the trivial solution ($c_\beta=d_\beta=b_\alpha=g_\alpha=0$) is avoided. The simplest method is to use a two-step approach: first, the energy is varied until the condition $\det(M)=0$ is satisfied, yielding the bound state energy E_b [41]; second, the wave function coefficients are calculated using this E_b and adding an arbitrary constraint, e.g., $c_{0,n_y}=0.25$, to Eq. (10), where n_y is the quantum number corresponding to the bound state located at E_b. This extra equation results in an overdetermined system which, when solved with a least-squares procedure, finds the nontrivial solution. In essence, the equation $c_{0,n_y}\neq 0$ acts as an arbitrary wave function normalization.

It should be noted that, due to the exponential terms of the strongly closed channels, using double-precision arithmetic it is impossible to locate the exact energy E_b at which $\det(M)=0$. Instead, the energy is scanned for the location at which there is a dip in $\det(M)$ over a few orders of magnitude. The bound state calculations were validated by reproducing the results for 2D hard walled circular electron waveguides with varying ϕ_0 and ρ_0 [41,43,44,46]. For the 3D SHO 90° bend with $\rho_0=4\pi$ (with $N_\alpha=10\times 3$ modes), the lowest three bound states were located at $E_b=0.899\,903\,451\,8$, $1.699\,903\,451\,8$, and $2.499\,903\,451\,8$, which gives the same binding energy $0.000\,096\,548\,2$ relative to each of their lowest propagation thresholds as expected. The 3D bend with SHO confinement, and only a single channel included in the calculation, gives binding by an energy of $0.000\,102\,685\,9$. A small amount of mode coupling is thus needed to describe the circular bend bound states due to the interface mismatching in Eq. (8) between $\varphi_{n_\rho}(\rho)$ and the SHO lead eigenfunctions of $\zeta_{n_x}(x)$.

The E_b that minimizes $\det(M)$ also corresponds exactly to the energy at which the least-squares residual of the matrix

M (supplemented with $c_{0,n_y}=0.25$) is the smallest. It is observed that the coefficients (b_α and g_α) become equal at this energy, consistent with a bound state of even symmetry about the midpoint of the bend at $\phi=\phi_0/2$. For the 3D SHO 90° bend with $\rho_0=4\pi$ the probability density of the $n_y=0$ bound state through a $y=0$ slice can be seen in Fig. 3. Since the binding energy is so small, the bound state extends a long way into the leads—which is the basis of the *infinite* leads assumption. However, the transverse profile of the wave function shown in Fig. 3 is consistent with the dominant mode being $n_x=0$.

These results can be contrasted with those given by a simple approximation. It has been demonstrated that a circular bend can be approximated by a ''straight,'' attractive, finite square well in the direction of propagation [39,42]. Defining the bend curvature as $\mathcal{C}=\phi_0/z_0=1/\rho_0$ (where the bend length $z_0=\rho_0\phi_0$), the effective square bend potential is given in Cartesian coordinates by

$$V_{\rm II}(x,y,z)=\frac{1}{2}m\omega^2[(x-\rho_0)^2+\lambda_y^2y^2]-\frac{\mathcal{C}^2}{8},\quad 0\leqslant z\leqslant z_0. \tag{12}$$

Furthermore, given that the angle of the bends under consideration is less than 360°, the approximate attractive finite square well supports only one bound state [43], and simple (transcendental) expressions for the bound state energy can be applied [42,47]. Numerically locating the unknown momentum q inside the potential well from

$$\sqrt{\frac{2m|V_z(z)|}{\hbar^2}-q^2}=q\tan\left(\frac{qz_0}{2}\right) \tag{13}$$

gives the bound state energy from $q^2=2m\{|V_z(z)|-E_b\}/\hbar^2>0$. This approximate model for the $\phi_0=90°$ bend with $\rho_0=4\pi$ results in $qz_0/2=0.366\,610$, giving a binding energy of $0.000\,101\,7$. As further program validation, the same attractive square well potential was run, giving $0.000\,101\,704\,7$ relative to the mode (0,0) threshold of $E=0.9$ [there is no mode coupling in this model, so a single ($N_\alpha=1\times1$) channel calculation suffices].

Leboeuf and Pavloff [37] have applied the single-channel square well model to study bound states of many interacting atoms in a bend. Using the Gross-Pitaevskii equation, they showed that in the presence of atom-atom interactions a bound state still exists. Given typical experimental parameters they further estimated the number of ^{87}Rb atoms that such circular bends can support in the bound state to be of the order of 7–70. Since the present method explicitly assumes no atom-atom interactions, it is beyond the scope of this work to verify their results.

C. Scattering (transmission, reflection, and mode-transfer)

Figures 4 and 5 display the core results of this paper; the transmission and reflection probabilities of the 90° bend with $\rho_0=4\pi$ at low energies $0.9<E<5.0$. While there are 16 modes energetically allowed at the end of this energy range, here the focus is on when the incoming matter wave is initially in the ground state, with the transmission probabilities for the (0,0) mode given in Fig 4(a). Transmission probabilities for the first two excited states as the incoming modes are also given; the (1,0) mode results are also shown in Fig. 4(a), while the (0,1) mode results are shown separately in Fig. 4(b). Note that for these calculations $N_\alpha=10\times2$.

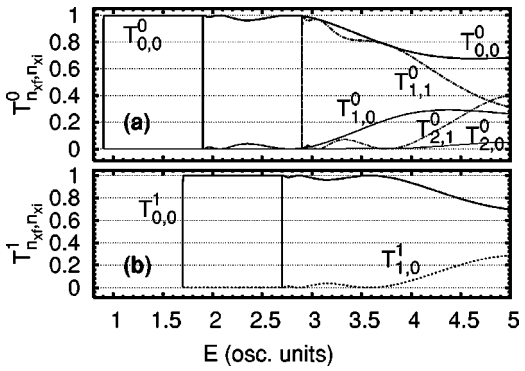

FIG. 4. Transmission and mode-conversion probabilities $T^{n_y}_{n_{xf},n_{xi}}$ for a 90° SHO bend with $\rho_0=4\pi$ as a function of energy (in oscillator units). The incoming (n_x,n_y) modes are restricted to the three lowest-energy modes given in Table II, with the (0,0) and (1,0) modes shown in (a), and the (0,1) mode shown separately in (b). Of primary interest is the transmission probability $T^0_{0,0}$, which is the probability of entering in the $(n_{xi}=0,n_y=0)$ ground state mode, and exiting in the same mode $(n_{xf}=0,n_y=0)$.

The important line in Fig. 4(a) is the $T^0_{0,0}$ result, that is, the probability of a ground state (0,0) matter wave propagating through the bend and exiting in the same ground state mode. At $E=4.9$, the mode (4,0) becomes energetically accessible, thus over the energy range seen in Figs. 4 and 5 there are four other lead modes that mode (0,0) can couple with. From the threshold of mode (0,0) propagation at $E=0.9$, $T^0_{0,0}$ rapidly rises to perfect transmission as the energy is increased. Unit transmission is predictably maintained while the energy remains below the threshold of the first accessible excited mode (1,0) at $E=1.9$. As the energy is

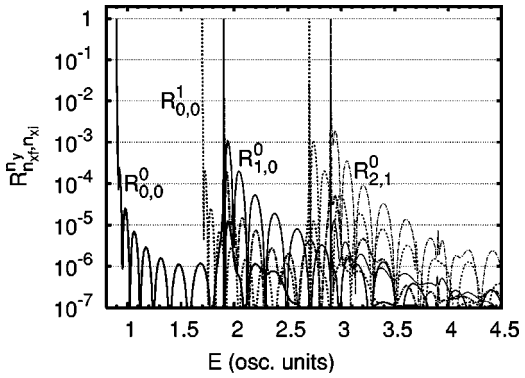

FIG. 5. Reflection probabilities $R^{n_y}_{n_{xf},n_{xi}}$ for a 90° SHO bend with $\rho_0=4\pi$ as a function of energy (in oscillator units). The incoming (n_x,n_y) modes are restricted to the lowest three modes given in Table II. Apart from threshold and resonant spikes, all reflection probabilities are significantly smaller than the corresponding transmission probabilities seen in Fig. 4.

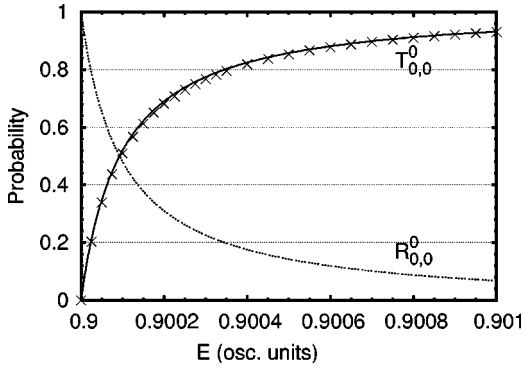

FIG. 6. Transmission $T^0_{0,0}$ and reflection probabilities $R^0_{0,0}$ for a 90° SHO bend with $\rho_0=4\pi$ at energies just above the mode (0,0) propagation threshold at $E=0.9$ (all energies in oscillator units). The crosses are the transmission probabilities given by Eq. (14) resulting from approximating the circular bend with the attractive square well potential of Eq. (13).

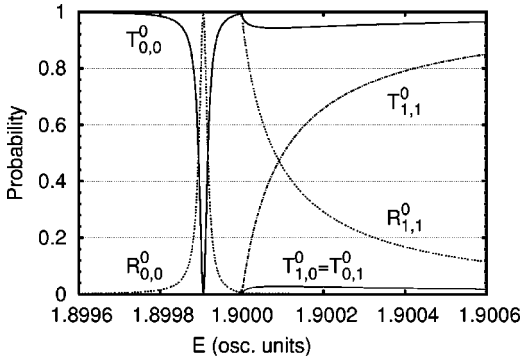

FIG. 7. Transmission $T^{n_y}_{n_{xf},n_{xi}}$ and reflection probabilities $R^{n_y}_{n_{xf},n_{xi}}$ for a 90° SHO bend with $\rho_0=4\pi$ at energies surrounding the mode (1,0) propagation threshold at $E=1.9$ (all energies in oscillator units). Mode (0,1) is not shown as it is unaffected by the presence of the $n_y=0$ modes.

increased above $E=1.9$, a small oscillation due to mode transfer can be seen in $T^0_{1,0}$. Once the third mode (2,0) becomes energetically open at $E=2.9$, $T^0_{0,0}$ decreases more sharply, primarily because of the mode transfer seen in the increase of $T^0_{2,1}$ and to a lesser extent in $T^0_{3,1}$. To demonstrate that mode transfer remains a small effect below the third mode threshold, other bend parameters are examined later.

Importantly, though, the reflection probabilities for the $n_y=0$ and $n_y=1$ modes shown in Fig. 5 are generally insignificant across the entire energy range, suggesting that mode transfer is the dominant source of loss from single-mode propagation at low energies. These results for the 3D SHO waveguide potential are consistent with previous investigations of ballistic 2D electron propagation through bends where the walls are ''soft'' [46]. In that study, instead of the confining potential suddenly going to an infinite value, it was found that even a large but finite potential waveguide wall reduces the amount of both reflection and mode mixing.

Another feature seen in both Figs. 4 and 5 is the similarity in the transmission and reflection probability of maintaining propagation in the ground $(n_x=0)$ state of each n_y mode. $T^1_{0,0}$, for example, exhibits the same characteristic change with energy as $T^0_{0,0}$. Both rapidly rise to unity as the energy is increased above their respective propagation thresholds. However, the probability of mode transfer by the bend becomes substantial at energies where two higher modes are energetically open to the incoming wave. This supports the result that, with n_y as a good quantum number, the physics of the 3D circular bend can effectively be considered as a 2D problem.

D. Thresholds and resonances

The sharp resonance spikes in the transmission and reflection probabilities seen in Figs. 4 and 5 near the thresholds of propagation are examined in depth in this section. Many of the features characterized for the case of 2D electron transport [42–44], such as the behavior near mode thresholds as well as the characteristics of the resonances, apply here.

The behavior of the transmission and reflection probabilities near the ground state propagation threshold can be seen in Fig. 6, with the transmission probability rapidly rising to unity from the $E=0.9$ threshold. Also included as the crosses on Fig. 6 are calculations resulting from approximating the bend with the attractive square potential of Eq. (12). These are calculated using the incoming propagation energy of the ground state wave, $E_k=E-E_{(n_x=1)}-E_{(n_y=1)}$, then $k^2=2mE_k/\hbar^2$ and $q^2=2m[E_k+|V_z(z)|]/\hbar^2$. The single-channel transmission probability can then be written as [42,47]

$$T^0_{0,0}=\frac{(2kq)^2}{(2kq)^2\cos^2(qz_0)+(q^2+k^2)^2\sin^2(qz_0)}. \quad (14)$$

The results of this approximation in Fig. 6 clearly demonstrate that the simple 1D approximation to the bend reproduces the physics of the bend remarkably well while the energy of the bend is such that there is only a single open channel in the leads.

Despite $T^0_{0,0}$ rapidly reaching unity from threshold, there are minor resonant oscillations while the energy is still in the single-channel regime. These oscillations are best seen in the reflection probabilities of both $R^0_{0,0}$ and $R^1_{0,0}$ of Fig. 5 below their first excitation thresholds. These oscillations correspond to those resulting from the sinusoidal terms in Eq. (14). Generally, wave scattering from an attractive 1D square well potential results in such resonances, where perfect transmission occurs when the width of the well matches an integral or half-integral number of de Broglie wavelengths in the well [47,48].

The transmission and reflection probabilities near the mode (1,0) threshold $(E=1.9)$ are shown in Fig. 7. The behavior of $T^0_{1,1}$ shows a smooth increase from threshold toward unity. The energy range also covers the resonance just below this threshold where total reflection of mode (0,0) occurs. As was the case for the bound state energy, the positions of the resonances are above the bend threshold, but marginally below the lead threshold (see Table II). This resonance is thus a Feshbach resonance generated through the

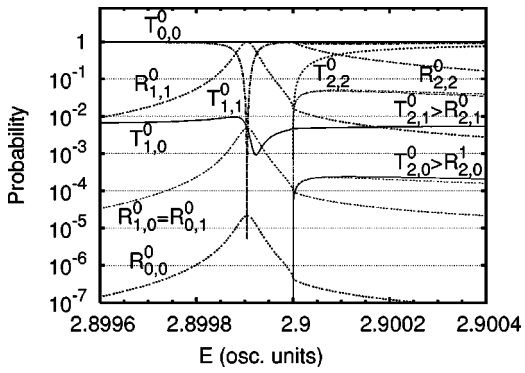

FIG. 8. Transmission $T^{n_y}_{n_{xf},n_{xi}}$ and reflection probabilities $R^{n_y}_{n_{xf},n_{xi}}$ for a 90° SHO bend with $\rho_0=4\pi$ at energies surrounding the mode (2,0) propagation threshold at $E=2.9$ (all energies in oscillator units). Due to symmetry the mode-transfer probabilities $T^0_{1,0}=T^0_{0,1}$, $R^0_{1,0}=R^0_{0,1}$, $T^0_{2,0}=T^0_{0,2}$, $R^0_{2,0}=R^0_{0,2}$, $T^0_{2,1}=T^0_{1,2}$, and $R^0_{2,1}=R^0_{1,2}$. The $n_y=1$ modes are not shown since they are unaffected by the presence of the $n_y=0$ modes.

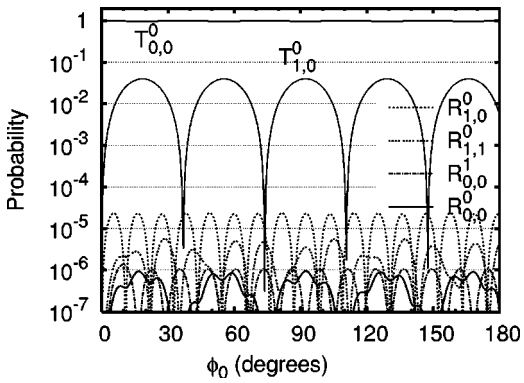

FIG. 9. Transmission $T^{n_y}_{n_{xf},n_{xi}}$ and reflection probabilities $R^{n_y}_{n_{xf},n_{xi}}$ for a SHO bend with $\rho_0=4\pi$ at a fixed energy $E=2.34$ (in oscillator units) as a function of bend angle ϕ_0 (in degrees). Only the lowest three modes in Table II are open at this energy. Note that $T^0_{1,0}\approx T^0_{0,1}$, and for mode (0,1) only $R^1_{0,0}$ is shown since $T^1_{0,0}\approx 1$.

coupling of the incoming propagating mode to the (1,0) mode—which is energetically open in the bend, but closed in the leads. Note that, due to its different quantum number, the (0,1) mode—while it is open throughout this energy range—is unaffected by the action related to modes with $n_y=0$, and is not shown in Fig. 7.

The resonance and mode transfer ($T^0_{1,0}$) effects seen in Fig. 7 cannot be seen in models based on the simple attractive square well potential of Eq. (12). This model completely ignores mode mixing since it uses the same transverse oscillation frequency in the bend as in the lead. The wave simply propagates faster in the bend, which is an adequate approximation at single-channel energies. For a realistic circular bend, at higher energies the wave propagates at increasingly further distances from the SHO minima, resulting in an increased mismatching of the lead-bend eigenfunctions and thus more mode transfer.

The behavior near the mode (2,0) threshold at $E=2.9$ can be seen in Fig. 8. The Feshbach resonance of $T^0_{1,1}$, at which energy there is total reflection, indicates that mode (1,0) couples strongly with the (2,0) mode in the bend. Mode (0,0), however, is only slightly perturbed by the presence of mode (2,0) propagating in the bend, which corresponds to a slight increase in $R^0_{0,0}$ and $R^0_{1,0}$, and a variation in $T^0_{1,0}$. Above the (2,0) threshold, $T^0_{2,2}$ approaches unity with the same characteristic as that of modes (0,0) and (1,0) shown in Figs. 6 and 8. This small effect of the mode (2,0) threshold on mode (0,0), and the dominant mixing between adjacent modes, i.e., $T^0_{2,1}\gg T^0_{2,0}$, can both be understood in terms of the overlap of the interface wave functions; the mode (0,0) wavefunction in the lead only weakly overlaps with mode (2,0) in the bend. Since there is no mode coupling within the waveguide, all of the mode mixing occurs through this matching.

The energy width of these Feshbach resonances is so small that it may be extremely difficult to experimentally observe a dip in the transmission to zero with a wave packet that has a finite energy spread. As a theoretical side note, the exact energy position of the resonances also corresponds to the energy where $\det(M)$ of Eq. (10) has a minimum.

E. Dependance on waveguide geometry

In this final section, the dependence of transmission on both angle and curvature is examined. The effects of varying bend parameters for the 2D electron waveguide has been investigated by Sols and Macucci [41]. In particular, their results relating the low-energy transmission probability to different bend angles and curvatures are qualitatively seen here.

To demonstrate the effects of varying the bend angle on the transmission and reflection probabilities, we again use a circular bend with $\rho_0=4\pi$. Both the lead and bend propagation energies seen in Table II remain constant as the angle is varied. It is, however, worthwhile to restrict the energy to below that of the mode (2,0) threshold (at $E=2.9$), so that only two propagating modes couple. Figure 9 shows transmission, reflection, and mode-conversion probabilities for a SHO bend at a fixed $E=2.34$ (with $N_\alpha=10\times 2$ modes), which was chosen to be near the local maximum of the mode transfer probability $T^0_{1,0}$ seen in Fig. 4. As expected, at $\phi_0=0°$ there is perfect transmission (i.e., there is no bend). At all angles, reflections continue to play an insignificant role compared to the mode transfer probability $T^0_{1,0}$, which displays periodic oscillation. Depending on the bend angle, mode conversion reaches a maximum of 4%, demonstrating that, in general, mode transfer remains a small effect while the energy of the incoming wave remains below the mode (2,0) threshold.

When only two channels couple, the critical angles ϕ_c at which the $T^0_{1,0}$ mode-conversion minima occur can be predicted by requiring that the mode (0,0) and (1,0) path lengths coincide:

$$(\kappa_{(0,0)}-\kappa_{(1,0)})\phi_c=2\pi n, \tag{15}$$

with $n=0,1,2,\ldots$. For the above geometry with $E=2.34$, using the computed values $\kappa_{(0,0)}=21.424$ and $\kappa_{(1,0)}$

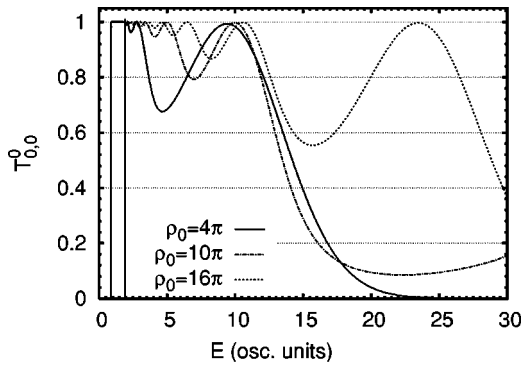

FIG. 10. Ground state mode (0,0) transmission probabilities $T^0_{0,0}$ for 90° SHO bends with different radii of curvature ρ_0 as a function of energy (in oscillator units). Virtually all of the ''loss'' in transmission is due to the transmission of excited modes $T^0_{n_{xf},0}$ where $n_{xf}>0$.

$=11.665$, this estimate gives $\phi_c=0°,36.89°,73.78°,110.7°,\ldots$ in agreement with the positions of the $T^0_{1,0}$ minima shown in Fig. 9. Furthermore, using a simple approximation for the bend kinetic energy, i.e., $\kappa^2_{(n_\rho,n_y)} \approx 2\rho_0^2(E-E_{(n_\rho,n_y)})$, along with the bend thresholds given by Table II, gives $\phi_c=0°,37.8°,75.5°,113.3°$, in reasonable agreement with Fig. 9.

Finally, and perhaps most relevant to experiments, Fig. 10 shows the transmission probability of the ground state mode for a $\phi_0=90°$ bend with the radius of curvature varied between the relatively tight bend used throughout this paper ($\rho_0=4\pi$), an intermediate bend ($\rho_0=10\pi$), as well as a longer bend ($\rho_0=16\pi$). The energy range was also extended well beyond that of Fig. 4, up to a maximum of $E=30$. Numerical convergence with such a large number of channels energetically open (484 channels at $E=30$) required the inclusion of $N_\alpha=25\times1$ channels, since only $n_y=0$ modes are of interest.

At low energies, the behavior of the transmission probability for all curves is virtually identical, with the different positions of the $T^0_{0,0}$ resonances unable to be discerned in Fig. 10. Above the mode (2,0) threshold at $E=2.9$, there are differences in both the phase and amplitude of the $T^0_{0,0}$ oscillations. As the energy is increased, the two tightest bends resulted in near 100% mode transfer around $E\approx20$, and even for the large $\rho=16\pi$ bend there is a significant amount of loss through mode transfer in this energy range. As expected, the longer the bend, the more adiabatic is the leap across the lead-bend interface. Even for large bends, however, the discontinuity still impacts the amount of mode transfer at high energies. This complete saturation of mode transfer for all of these bends is not only due to the large number of open channels at these high energies; returning to Fig. 2, as the energy is increased to such high energies, the maximum of the mode (0,0) eigenfunction in the bend is located a long distance from $\rho=\rho_0$. There is furthermore almost no overlap of the $E=27$ eigenmode with the center of the waveguide, resulting in complete mismatching at the lead-bend interfaces, leaving no chance of single-mode transmission. Although it is not shown here, it should again be emphasized that reflections continue to play a minor role in the wave propagation dynamics at energies above the mode (0,2) threshold for all these different bend geometries.

IV. CONCLUSIONS

We have shown how to apply the time-independent quantum mode-matching method to describe the physics of noninteracting low-energy atom waves propagating through circular bends. Explorations of the transmission, reflection, and mode-transfer probabilities for different bends over a wide range of energies have found that, while single-mode wave propagation indeed dominates at low energies, at higher energies excitation and transmission of other modes are possible. Significantly for ''atom chip'' designers, reflections are generally negligible even for sharply curved bends.

Matching the bend eigenfunctions to the lead eigenfunctions across the effective discontinuity at the interfaces is problematic, even for the long bends. It is likely that to obtain true ''adiabatic'' wave-packet transport through waveguide bends, atom chip microstructures should be designed with a gradual transition from the leads into and out of the bend. With the recent experimental successes of BEC creation and controlled propagation above microchip surfaces, investigations in the regime of propagation velocities comparable in energy to the transverse excitation energies should also avoid many of the manifestations of mode transfer examined here.

A majority of the 3D circular bend SHO waveguide results demonstrated here are qualitatively similar to those well known in the context of electromagnetic waveguides and ballistic electron transport through quantum wires. The present paper highlights that the same rich array of physics, such as bound states and Feshbach resonances, will also impact ultracold atom propagation through waveguides. However, as a dampening note, the direct experimental observation of an energetically narrow resonant dip in the wave transmission that was observed over ten years ago with electromagnetic waveguides [49] may prove to be extremely difficult with a matter wave packet propagating through a bend.

The present results emphasizing conditions for single-mode wave propagation through circular bends can also provide some insight into current ultracold atom investigations, e.g., BEC propagation past a spatial defect in the waveguide [36], or the propagation of atoms around a stadium with straight sides and circular bends [50], where bound states and interface discontinuities may occur. The extension of the present time-independent method to treat such geometries is eminently feasible. Furthermore, imperfections and interatomic collisions provide a mechanism for mode transfer, and a time-dependent wave-packet approach that can include atom-atom interactions is probably of more interest for present experimental configurations. Both of these theoretical approaches would also enable the examination of more complicated and unusual atom chip devices.

ACKNOWLEDGMENTS

This work was supported by the Department of the Navy, Office of Naval Research, and by the Research Corporation.

[1] R. Folman, P. Krüger, J. Schmiedmayer, J. Denschlag, and C. Henkel, Adv. At., Mol., Opt. Phys. **48**, 263 (2002).
[2] E.A. Hinds and I.G. Hughes, J. Phys. D **32**, R119 (1999).
[3] J.P. Dowling and J. Gea-Banacloche, Adv. At., Mol., Opt. Phys. **37**, 1 (1996).
[4] G. Birkl, F.B.J. Buchkremer, R. Dumke, and W. Ertmer, Opt. Commun. **191**, 67 (2001).
[5] J. Reichel, W. Hänsel, P. Hommelhoff, and T.W. Hänsch, Appl. Phys. B: Lasers Opt. **72**, 81 (2001).
[6] L. Feenstra, L.M. Andersson, and J. Schmiedmayer, e-print cond-mat/0302059v2.
[7] P. Berman, *Atom Interferometry* (Academic Press, San Diego, 1997).
[8] J. Schmiedmayer, Appl. Phys. B: Lasers Opt. **60**, 169 (1995).
[9] J. Schmiedmayer, Phys. Rev. A **52**, R13 (1995).
[10] J.D. Weinstein and K.G. Libbrecht, Phys. Rev. A **52**, 4004 (1995).
[11] J.H. Thywissen, M. Olshanii, G. Zabow, M. Drndić, K.S. Johnson, R.M. Westervelt, and M. Prentiss, Eur. Phys. J. D **7**, 361 (1999).
[12] T.J. Davis, J. Opt. B: Quantum Semiclassical Opt. **1**, 408 (1999).
[13] J.P. Burke, Jr., S. Chu, G.W. Bryant, C.J. Williams, and P.S. Julienne, Phys. Rev. A **65**, 043411 (2002).
[14] C. Henkel and S. Pötting, Appl. Phys. B: Lasers Opt. **72**, 73 (2001).
[15] C. Henkel, P. Krüger, R. Folman, and J. Schmiedmayer, Appl. Phys. B: Lasers Opt. **76**, 173 (2003).
[16] C. Henkel and S.A. Gardiner, e-print cond-mat/0212415v2.
[17] M. Jääskeläinen and S. Stenholm, Phys. Rev. A **66**, 023608 (2002).
[18] M. Jääskeläinen and S. Stenholm, Phys. Rev. A **66**, 043612 (2002).
[19] V.V. Klimov and V.S. Letokhov, JETP Lett. **70**, 666 (1999).
[20] J.H. Thywissen, R.M. Westervelt, and M. Prentiss, Phys. Rev. Lett. **83**, 3762 (1999).
[21] E. Andersson, T. Calarco, R. Folman, M. Andersson, B. Hessmo, and J. Schmiedmayer, Phys. Rev. Lett. **88**, 100401 (2002).
[22] M.D. Girardeau, K.K. Das, and E.M. Wright, Phys. Rev. A **66**, 023604 (2002).
[23] J.A. Stickney and A.A. Zozulya, Phys. Rev. A **66**, 053601 (2002).
[24] D.C.E. Bortolotti and J.L. Bohn, e-print physics/0309003.
[25] J.A. Stickney and A.A. Zozulya, Phys. Rev. A **65**, 053612 (2002).
[26] M. Jääskeläinen and S. Stenholm, Phys. Rev. A **66**, 053605 (2002).
[27] P. Horak, B.G. Klappauf, A. Haase, R. Folman, J. Schmiedmayer, P. Domokos, and E.A. Hinds, Phys. Rev. A **67**, 043806 (2003).
[28] D. Müller, D.Z. Anderson, R.J. Grow, P.D.D. Schwindt, and E.A. Cornell, Phys. Rev. Lett. **83**, 5194 (1999).
[29] N. Blanchard and A. Zozulya, Opt. Commun. **190**, 231 (2001).
[30] W. Hänsel, P. Hommelhoff, T.W. Hänsch, and J. Reichel, Nature (London) **413**, 498 (2001).
[31] H. Ott, J. Fortagh, G. Schlotterbeck, A. Grossman, and C. Zimmermann, Phys. Rev. Lett. **87**, 230401 (2001).
[32] A. Kasper, S. Schneider, C. vom Hagen, M. Bartenstein, B. Engeser, T. Schumm, I. Bar-Joseph, R. Folman, L. Feenstra, and J. Schmiedmayer, J. Opt. B: Quantum Semiclassical Opt. **5**, S143 (2003).
[33] S. Schneider, A. Kasper, C. vom Hagen, M. Bartenstein, B. Engeser, T. Schumm, I. Bar-Joseph, R. Folman, L. Feenstra, and J. Schmiedmayer, Phys. Rev. A **67**, 023612 (2003).
[34] J. Fortágh, H. Ott, S. Kraft, A. Günther, and C. Zimmermann, Appl. Phys. B: Lasers Opt. **76**, 157 (2003).
[35] T.L. Gustavson, A.P. Chikkatur, A.E. Leanhardt, A. Görlitz, S. Gupta, D.E. Pritchard, and W. Ketterle, Phys. Rev. Lett. **88**, 020401 (2002).
[36] A.E. Leanhardt, A.P. Chikkatur, D. Kielpinski, Y. Shin, T.L. Gustavson, W. Ketterle, and D.E. Pritchard, Phys. Rev. Lett. **89**, 040401 (2002).
[37] P. Leboeuf and N. Pavloff, Phys. Rev. A **64**, 033602 (2001).
[38] P. Exner and P. Seba, J. Math. Phys. **30**, 2574 (1989).
[39] J. Goldstone and R.L. Jaffe, Phys. Rev. B **45**, 14100 (1992).
[40] M. Andrews and C.M. Savage, Phys. Rev. A **50**, 4535 (1994).
[41] F. Sols and M. Macucci, Phys. Rev. B **41**, 11887 (1990).
[42] D.W.L. Sprung, H. Wu, and J. Martorell, J. Appl. Phys. **71**, 515 (1992).
[43] K. Lin and R.L. Jaffe, Phys. Rev. B **54**, 5750 (1996).
[44] O. Olendski and L. Mikhailovska, Phys. Rev. B **66**, 035331 (2002).
[45] R.L. Schult, D.G. Ravenhall, and H.W. Wyld, Phys. Rev. B **39**, 5476 (1989).
[46] C.S. Lent, Appl. Phys. Lett. **56**, 2554 (1990).
[47] S. Gasiorowicz, *Quantum Physics* (Wiley, New York, 1974).
[48] B.H. Bransden and C.J. Joachain, *Introduction to Quantum Mechanics* (Longman, Essex, England, 1989).
[49] J.P. Carini, J.T. Londergan, K. Mullen, and D.P. Murdock, Phys. Rev. B **46**, 15538 (1992).
[50] W. Rooijakkers, S. Wu, and M. Prentiss (unpublished).